# Thermal Self-Protection of Zinc-Ion Batteries Enabled by Smart Hygroscopic Hydrogel Electrolytes

*Peihua Yang, Chunzao Feng, Yipu Liu, Ting Cheng, Xuelong Yang, Huidong Liu, Kang Liu,* and Hong Jin Fan**

Dr. P. Yang, Dr. Y. Liu, Prof. H. J. Fan
School of Physical and Mathematical Sciences, Nanyang Technological University, Singapore, 637371, Singapore
E-mail: fanhj@ntu.edu.sg

C. Feng, Dr. T. Cheng, Dr. X. Yang, Dr. H. Liu, Prof. K. Liu
MOE Key Laboratory of Hydraulic Machinery Transients, School of Power and Mechanical Engineering, Wuhan University, Wuhan, Hubei 430072, China
E-mail: kang.liu@whu.edu.cn

Prof. H. J. Fan
Innovative Centre for Flexible Devices, Nanyang Technological University, Singapore, 639798, Singapore

**Abstract**: Efficient thermal protection is essential to battery safety. Here, a self-adaptive strategy is demonstrated to circumvent the thermal runaway of aqueous zinc-ion batteries, by using zinc chloride-enriched hygroscopic hydrogel electrolyte. At high temperatures, water inside the hydrogel can quickly evaporate to dissipate the heat generated. Concurrently, excessive water evaporation causes a sudden drop in the ion diffusion of the hydrogel electrolyte, thereby effectively restricting the migration of ions and shut down the battery. When the temperature lowers, the hydrogel absorbs water from the ambient and the battery recovers its function. The evaporation and regeneration of water in the hydrogel electrolytes are highly reversible, thus realizing intelligent and efficient thermal self-protection of zinc-ion batteries. By properly designing and engineering the hygroscopic hydrogel electrolytes, it is believed that other thermal self-protective aqueous batteries with faster response can be accomplished, which shows promise for safe power supply in both consumable electronics and electric vehicles.

*Keywords: zinc-ion battery, thermal self-protection, hygroscopic hydrogel, intelligent*

With the fast development of digital society, advanced batteries with high energy density and high-power delivery, and more importantly, high safety, are in great demand for wireless communications, transportation, personal electronics, and so on.[1-3] These batteries generate considerable joule heat during fast charging/discharging,[4-5] resulting in a local high temperature environment. High operation temperature may cause permanent performance degradation of the batteries, or even lead to explosion and fire risks.[6] Therefore, thermal runaway of high energy and power densities batteries is increasingly becoming a serious safety issue, and effective thermal runaway control is of great significance.[7-8] Traditional strategy to mitigate thermal runaway heavily relies on an external thermal management system, which cools down the batteries by fans[9] or flow liquids.[10] The extra accessories not only consume additional energy, but also increase the complexity and footprint of the system. Moreover, if the thermal management system becomes invalid in extreme cases, the batteries will remain completely unprotected and at high fire risk. Recently, smart batteries with the function of thermal self-protection emerges as an attractive strategy to achieve operation safety.[11-12]

Thermal self-protection requires the battery to self-lock down at high temperatures and recover to working state when the battery cools down. Thermoresponsive polymer electrolytes with the function of sol-gel transition have been proved an important approach to implement in thermal self-protection.[13-16] These electrolytes change from liquid state to gel when the temperature goes beyond the transition-temperature (~50 °C), thus suppressing the ions transport inside the battery.[17-18] However, the thermoresponsive polymer electrolytes still allow considerable ion mobility in gel state, so that the electrolytes reduce but do not cut off the ion transport at high temperatures. Hence, the battery will not be deactivated completely, but works at a notable capacity,[13] limiting the efficiency of thermal self-protection.

Compared with lithium-ion batteries, aqueous zinc-ion batteries have advantages of low cost and high theoretical capacity of zinc electrode.[19-24] Because of the high energy and high power delivery capability of zinc-ion batteries, considerable joule heat may be generated and may

cause safety issues. In addition, thermal runaway of batteries can be triggered by various external reasons, such as extreme temperature, mechanical abuse and electrical abuse. Among various methods, thermal-responsive electrolytes are proved effective in mitigating this issue.[25-26] Here we propose a new strategy using smart hygroscopic hydrogel electrolytes to achieve efficient thermal self-protection of zinc-ion batteries (see schematic in **Figure 1**). We first characterize the thermal response of the hydrogel followed by implementing the hydrogel electrolytes in a full Zn/$MnO_2$ battery. It is shown that the Zn/$MnO_2$ battery spontaneously reduces their capacity to almost zero when it is heated to temperatures beyond 50 °C, and gradually resumes the initial capacity when the device cools down. Our proof-of-concept demonstration may inspire new strategies to promote thermal self-protection of zinc-ion batteries as well as other aqueous electrochemical energy devices.

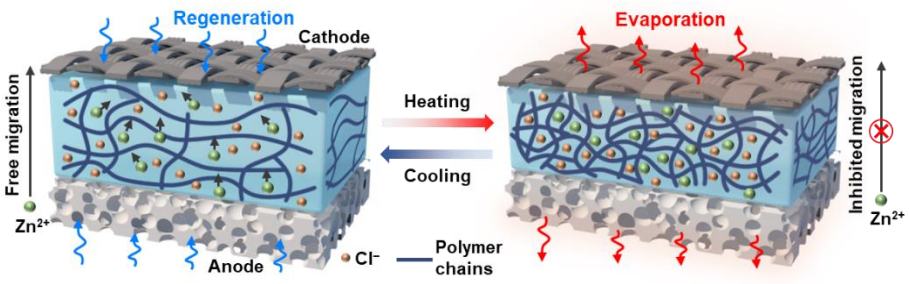


**Figure 1**. Working principle of the thermal self-protective zinc-ion batteries based on hygroscopic hydrogel electrolyte.

Figure 1 illustrates the structure and working principle of the thermal self-protective zinc-ion battery. Porous zinc foam and $MnO_2$/carbon cloth fiber are used as the anode and cathode, respectively. Morphology and XRD patterns of the electrode materials are shown in Figure S1 and Figure S2. The hydroscopic hydrogel electrolyte was prepared with polyacrylamide (PAAm) hydrogel as solid frame filled with $ZnCl_2$ solution (denoted as Zn-PAAm). Here $ZnCl_2$ solution is employed for two reasons: first, it is a commonly used low-cost electrolyte for zinc-ion batteries;[27] second, the saturated vapor pressure of $ZnCl_2$ solution can be easily regulated by its concentration (Figure S3).[28] The strong ability of $ZnCl_2$ solution in vapor pressure manipulation endows the batteries two intelligent characteristics in response to thermal shock

as follows. First, when the battery encounters a thermal shock, water in the electrolyte spontaneously evaporates through the porous electrodes to dissipate large amount of heat, thereby alleviating the local high temperature. Moreover, as the water evaporates, the ions transport in the hydrogel between Zn anode and $MnO_2$ cathode will gradually be restricted until completely cut off. The battery accordingly stops working and achieves thermal self-protection at high temperature. When the battery cools down, the hydrogel electrolyte spontaneously absorbs water from the surrounding air and regenerates itself. Thus, the battery recovers to the initial state again. Such reversible moisture recycle lays a solid foundation for sustainable thermal self-protection of the batteries.

Before testing the performance of the zinc-ion battery, we characterized the basic properties of the smart hydrogel electrolyte. As shown in **Figure 2**a, the Zn-PAAm hydrogel is quite stable under ambient condition (25 °C and 70% RH). The mass of hydrogel remains almost unchanged within ten days, and no visible change in transparency or color can be found on the hydrogel even after three months. This new Zn-PAAm hydrogel electrolyte is more stable than traditional hydrogel materials; the latter are significantly dehydrated when exposed to the atmosphere for a short period of time.[29-30] From the thermogravimetric measurement result (Figure S4), the vaporizable water in the Zn-PAAm hydrogel accounts for 56% by weight of the total, indicating an equivalent free water volume fraction of ~92% in the hydrogel electrolyte. The high stability of water inside the hydrogel comes from the moisture equilibrium between the hydrogel and the surrounding environment.[31-32] At a temperature of 25 °C, the saturated vapor pressure of the hydrogel is 2.3 kPa, which is close to the partial pressure of vapor in ambient environment with the relative humidity of 70% (2.2 kPa), making the hydrogel stable under ambient condition. If the ambient humidity changes, the hydrogel will slightly change its concentration spontaneously to reach a new equilibrium.

Although the Zn-PAAm hydrogel maintains moisture equilibrium with the ambient environment, high temperature can easily break the balance. The saturated vapor pressure of

the hydrogel increases significantly with temperature (Figure 2b). Therefore, at high temperatures, rapid vapor evaporation occurs in the hydrogel. When the hydrogel was heated up to 50 °C, the hydrogel lost about 0.3 g to reach a new equilibrium with the environment (Figure 2c). When the temperature cooled to 25 °C, the Zn-PAAm hydrogel spontaneously absorbed water from the ambient air until the weight came to the initial value. This water evaporation and regeneration process shows good circulation and repeatability (Figure S5), which is essential for the reversibility and cycling of the batteries' thermal self-protection.

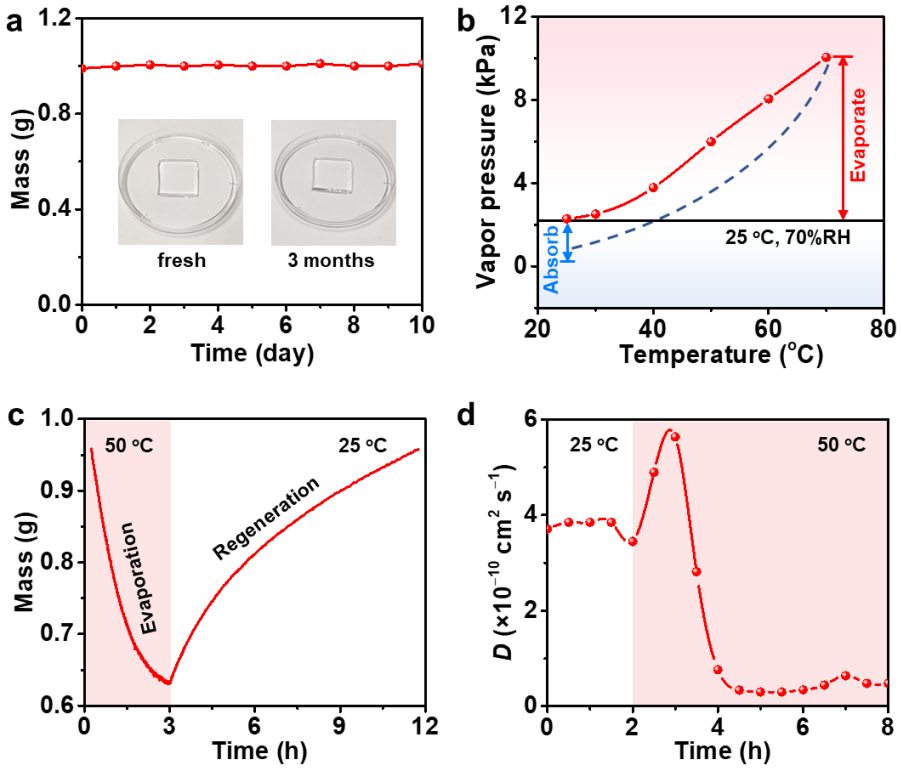


**Figure 2**. Basic characterizations of the Zn-PAAm hydrogel electrolyte. (a) Mass variation of the hydrogel when exposed in ambient environment (25 °C and 70% RH). The inset shows a piece of hydrogel after storage in laboratory air ambient for three months and a piece of newly prepared hydrogel. The size of the samples is 2 cm × 2 cm × 2 mm. (b) Saturated vapor pressure of the Zn-PAAm hydrogel at different temperatures. The black line indicates the partial pressure of vapor in ambient condition (2.2 kPa). (c) Mass change of the hydrogel at 50 °C and subsequent mass recovery at 25 °C. (d) Ion diffusion coefficient of the hydrogel electrolyte when the temperature increased from 25 °C to 50 °C.

During the water evaporation, the ion diffusion coefficient of the hydrogel electrolyte can be monitored by impedance spectroscopy[33-34] (Figure S6), and the results are shown in Figure 2d. When the temperature rose to 50 °C, water evaporated moderately at the beginning. The ion

diffusion coefficient inside the hydrogel increased due to thermal effect[35] and this process lasted about one hour. With further evaporation, water in the hydrogel was insufficient to support the effective transport of ions, and the ion diffusion coefficient significantly decreased. In the end, the ion diffusion coefficient was reduced by an order of magnitude, from $3.8 \times 10^{-10}$ to $3.4 \times 10^{-11}$ $cm^2$ $s^{-1}$. Meanwhile, the conductivity of the hydrogel electrolyte suffers from a remarkable decrease (Figure S7). The large decrease in ion diffusion coefficient and conductivity inhibits the migration of ions between anode and cathode. Hence, the temperature dependence of water content in the hydrogel, which then reversibly regulates the ions' migration in the hydrogel, is the working principle of the thermal self-protective batteries to be shown below.

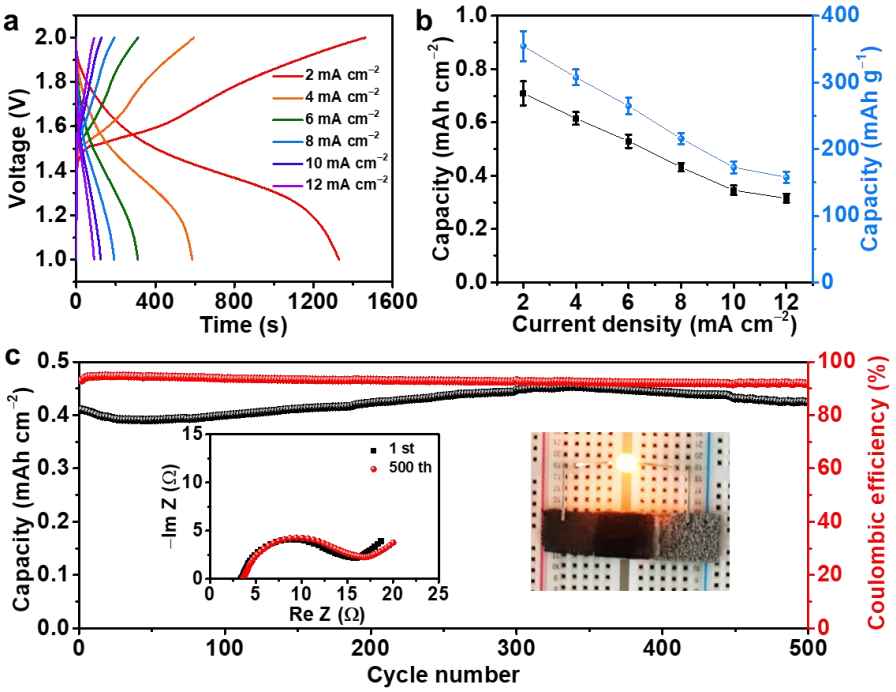


**Figure 3**. Electrochemical performance of zinc-ion batteries based on hygroscopic Zn-PAAm hydrogel electrolyte at ambient condition. (a) The charge and discharge curves under different current densities. (b) Areal capacity and gravimetric capacity calculated based on discharge curves. Statistical analysis is based on four similar samples. (c) Cycling stability test at 10 mA $cm^{-2}$. The insets show the battery impedance spectra and a photograph of a battery powering an orange light-emitting diode.

With the Zn-PAAm hygroscopic hydrogel electrolyte, we constructed a zinc-ion concept battery with porous zinc foam anode and $MnO_2$/carbon cloth fiber cathode. We tested the basic

electrochemical performance of the battery at ambient condition as shown in **Figure 3**. The galvanostatic charge and discharge profile indicates overlapped voltage plateaus of 1.2-1.8 V (Figure 3a), which are derived from protons and zinc ions co-insertion into the $MnO_2$ cathode.[36-37] The areal capacity and gravimetric capacity were determined from the discharge curves (see Figure 3b). At a current density of 2 mA $cm^{-2}$, the areal capacity is ~0.7 mAh $cm^{-2}$. The corresponding gravimetric capacity (based on $MnO_2$ loading) reaches ~370 mAh $g^{-1}$, which is comparable to previous Zn/$MnO_2$ batteries.[38-41] This zinc-ion battery is capable to power electronic devices, such as light-emitting diodes.

Compared with aqueous $ZnCl_2$ electrolyte, the Zn-PAAm hydrogel electrolyte shows highly stable Zn plating/stripping behavior (**Figure S8**), which can suppress the generation of zinc dendrites and enhance the cycling stability of batteries. As shown in Figure 3c, the Zn/$MnO_2$ battery with Zn-PAAm hydrogel electrolyte exhibits nearly no capacity decline at room temperature within 500 cycles, obviously better than the battery with aqueous $ZnCl_2$ electrolyte (**Figure S9**c). However, without thermal protection, the performance of batteries based on liquid and hydrogel electrolytes both decay sharply with cycling at 50 °C (**Figure S10 and S11**), which can be attributed to active materials loss and internal resistance increase due to the elevated temperature.[42] This result again emphasizes the importance of thermal protection for battery usage.

To demonstrate the thermal self-protection of the designed battery, we used external heating to simulate a high temperature environment (illustrated in **Figure 4**a). Two thermocouples were set on the electrodes to monitor the operation temperature (**Figure S12a**). The temperature of the battery surface was much lower than the given temperature of the heater (Figure 4b). When the heater was set at 70 °C, the temperature of $MnO_2$ cathode was 50.5 °C (Figure 4b). It is because water inside the hydrogel electrolyte evaporates through the porous $MnO_2$ electrode and takes heat away, achieving self-cooling function. To check the possible cooling effect due to thermal resistance of the battery (which also can lower the temperature), the battery was

sealed to eliminate evaporative cooling. As a result, the temperature of the cathode rose to 63 °C. Hence, it could be deduced that self-cooling from 63 to 50.5 °C originates from water evaporation.

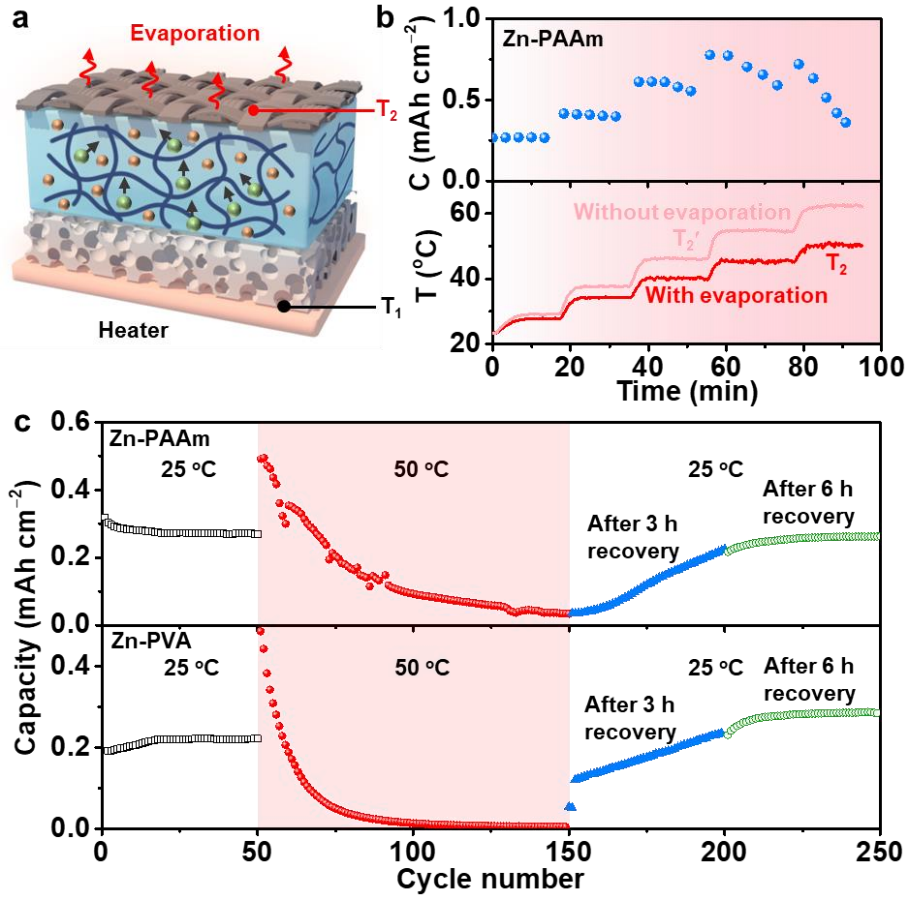


**Figure 4**. Demonstration of the thermal self-protection of zinc-ion batteries enabled by hygroscopic hydrogels electrolytes. (a) Schematic of the thermal runway experiment simulated by a heating plate. (b) The capacity variation of battery based on Zn-PAAm hydrogel electrolyte and temperature evolution of $MnO_2$ cathodes under transient heating with ($T_2$) and without ($T_2'$) evaporation. The temperature of heater ($T_1$) is increased from 30 to 70 °C with an interval of 10 °C. (c) The thermal-responsive reversibility of the zinc-ion batteries based on two types of hydrogel electrolytes: Zn-PAAm hydrogel (top panel) and Zn-PVA hydrogel (bottom panel). The capacity is derived from galvanostatic discharge measurement with a current density of 12 mA $cm^{-2}$.

In a short-time (up to 40 min) high temperature environment, the battery can maintain its capacity (see Figure 4b). The capacity even increases slightly because of the increased ion diffusion coefficient. That implies that battery can still be a temporary emergency power supply in a sudden thermal shock. However, if the battery is placed in high temperature for longer time

(e.g., after about 10 cycles in Figure 4c top panel), it starts to lock down with only negligible capacity output. When the heater resumes to room temperature, the hydrogel electrolyte absorbs water from ambient environment and the battery gradually recovers to work after 3 hours. And the capacity is nearly the same as the initial state, indicating good thermal self-protection of cell even with a period of transient capacity increase. Although the absorption of water by the hygroscopic electrolyte is an exothermic process, the electrode temperature is only ~0.5 $^{o}$C higher than the ambient temperature upon rehydration (Figure S12b), which can hardly produce significant negative thermal effects to the battery. The thermal response rate of the cell is still relatively low (~2 hours). This response rate of eletrolyte depends on the water evaporation rate, which is determined by a few factors, including size and shape of the hydrogel, porosity of the electrodes, and the vapor pressure difference between the sample and environment. It is posible to accelerate the evaporation rate with large explosure surface and in an environment with high temperature and low humidity. It is also worth noting that the PAAm polymer chain is not unique for the hygroscopic hydrogel electrolyte design. We also prepared polyvinyl alcohol (PVA) hydrogel using chemical crosslinking method,[43] and the thermal self-protection function of Zn-PVA electrolyte is similar to Zn-PAAm electrolyte (Figure 4c bottom panel and **Figure S13**). This proves that the hygroscopic hydrogel electrolyte is a general strategy for thermal self-protection of batteries.

In summary, we have presented an efficient thermal self-protection strategy for zinc-ion batteries by employing smart hygroscopic hydrogel electrolytes. The reversible water evaporation and regeneration process in the hydrogel are closely linked to the rise and fall of temperature, which can tune the migration of ions in the hydrogel. As a result, the hygroscopic hydrogel-based zinc-ion batteries display an evident thermal-responsive capability and realize efficient self-protection at high temperatures. Future research could push the thermal response and recovery speed by designing more advanced hydrogel molecules, which will provide new opportunities to thermal self-protection of aqueous batteries. Additionally, it is believed that

other type of thermal self-protective electrochemical storage devices can also be realized by properly introducing different metal ions in the hygroscopic hydrogel, towards more general applications in safe and controlled power delivery.

**Experimental Details**

*Preparation of Zn-PAAm hydrogel electrolyte*: The polyacrylamide (PAAm) hydrogel was prepared as previous literatures.[30-31] A precursor solution containing 2 mol $L^{-1}$ acrylamide (AAm), 0.001 mol $L^{-1}$ N,N′-methylenebis(acrylamide) and 0.002 mol $L^{-1}$ 2-hydroxy-4′-(2-hydroxyethoxy)-2-methylpropiophenone was prepared firstly. Then the solution was poured into a predetermined mold and irradiated with ultraviolet light (365 nm, ~4 mW $cm^{-2}$) for 4 hours under nitrogen protection to obtain PAAm hydrogel. The resulting hydrogel was completely swollen in deionized water and dried in oven at 60 °C until the hydrogel was dehydrated. Finally, the dehydrated hydrogel was soaked in 5.5 mol $L^{-1}$ $ZnCl_2$ solution until it swelled completely. The obtained hygroscopic hydrogel electrolyte is denoted as Zn-PAAm.

*Preparation of Zn-PVA hydrogel electrolyte*: The polyvinyl alcohol (PVA) hydrogel was prepared by chemical crosslinking method.[43] First, 10 wt% polyvinyl alcohol (PVA, Mowiol® PVA-117, Mw ~145,000) aqueous solution was prepared at 80 °C under stirring until the solution was clear. Subsequently, 5 mL PVA solution, 50 μL 1.2 mol $L^{-1}$ HCl and 50 μL glutaraldehyde (25% solution in water) were mixed and poured into a predetermined mold, and then placed in the hood overnight to obtain PVA hydrogel. The resulting hydrogel was completely swollen in deionized water and dried in oven at 60 °C until the hydrogel was dehydrated. Finally, the dehydrated hydrogel was soaked in 5.5 mol $L^{-1}$ $ZnCl_2$ until it swelled completely. The obtained hygroscopic hydrogel electrolyte is denoted as Zn-PVA.

*Preparation of $MnO_2$/carbon cloth fiber cathode*: The $MnO_2$ was deposited on the carbon cloth fiber by electrochemical method.[37] A homemade electrolysis cell with Zn plate and carbon cloth fiber was constructed. The electrolyte was a mixed solution of 1 mol $L^{-1}$ $ZnSO_4$, 1 mol $L^{-}$

[1] $MnSO_4$ and 0.1 mol $L^{-1}$ $H_2SO_4$. The cell was charged at 2.2 V to 2 mAh $cm^{-2}$ with a constant-voltage technique, and then discharge at a current density of 10 mA $cm^{-2}$. The charge/discharge process was conducted on Neware battery cycler and performed 20 cycles. The areal mass loading of $MnO_2$ on the carbon cloth was about 2 mg $cm^{-2}$.

*Fabrication of thermal self-protective zinc-ion batteries*: The battery was assembled by a piece of commercial zinc foam anode and as-prepared $MnO_2$/carbon cloth cathode. The hygroscopic hydrogel (1 cm × 1 cm × 0.5 mm) served as both electrolyte and separator. The electrochemical active area of the device was controlled at 1 $cm^2$. The battery was characterized directly in laboratory ambient condition (25 °C, 70% RH).

*Characterizations*: The morphology of the electrode materials was characterized by the scanning electron microscope (TESCAN, MIRA3). The X-ray diffraction test was performed by an X-ray diffractometer (TDM-10, Tongda). The thermogravimetric analysis of the hydrogel electrolyte was performed via a thermogravimetric analyzer (TGA 4000, PerkinElmer). Mass variations of hydrogel were measured by an electronic balance (ML-T, Mettler Toledo). Electrodes' temperature of the battery was measured using thermocouples (Omega Company) and recorded by a data logger (TC-08, Pico Technology). The electrochemical properties of the hydrogel electrolytes and batteries were obtained with an electrochemical workstation (CHI 660E). The battery cycling stability was conducted on Neware battery cycler (CT-4008T-5V50mA-164, Shenzhen, China).

*Calculations*: The vapor pressure of the hydrogel electrolytes was determined by using thermogravimetry method.[44] According to Langmuir equation, the vapor pressure can be expressed as:

$$-\frac{\mathrm{d}m}{\mathrm{d}t} = p\alpha\sqrt{\frac{M}{2\pi RT}}$$

where $-\mathrm{d}m/\mathrm{d}t$ is the rate of mass loss per unit area, $p$ is the vapor pressure, $\alpha$ is the vaporization coefficient, $M$ is the molecular weight of the effusing vapor, $R$ is the gas constant and $T$ is the

absolute temperature. Compared with water reference sample, the vapor pressure of the hydrogel electrolytes can be obtained:

$$p_{\mathrm{T}} = p_{\mathrm{Ref,T}} \frac{-(\mathrm{d}m/\mathrm{d}t)_{\mathrm{T}}}{-(\mathrm{d}m/\mathrm{d}t)_{\mathrm{Ref,T}}}$$

The conductivity ($\sigma$) of the hydrogel electrolyte can be calculated as:[26]

$$\sigma = \frac{d}{R_0 S}$$

where $d$ and $S$ are the thickness and area of hydrogel electrolyte, respectively. $R_0$ is the bulk resistance, which can be estimated on impedance spectra where the phase angle attains close to zero.

The ions diffusion coefficient can be calculated by Fick's law through impedance measurement:[33-34]

$$D = \frac{R^2 T^2}{2S^2 F^4 n^4 c^2 W^2}$$

where $R$ is the gas constant, $T$ is the absolute temperature, $S$ is the area of hydrogel electrolyte, $F$ is the Faraday constant, $n$ is the valence, $c$ is the ions concentration, and $W$ is the Warburg coefficient.

**Supporting Information**

Supporting Information is available from the Wiley Online Library or from the author.

**Acknowledgements**

P.Y. and C.F. contributed equally to this work. K.L. acknowledges the funding support from the National Natural Science Foundation of China (51976141). H.J.F. acknowledges the financial support from the Agency for Science, Technology, and Research (A*STAR) by AME Individual Research Grant (A1883c0004), and Ministry of Education by Tier 1 (RG157/19).

Received: ((will be filled in by the editorial staff))
Revised: ((will be filled in by the editorial staff))
Published online: ((will be filled in by the editorial staff))

References

[1] C. Xia, C. Y. Kwok, L. F. Nazar, *Science* **2018**, *361*, 777.
[2] L. Chen, X. Fan, X. Ji, J. Chen, S. Hou, C. Wang, *Joule* **2019**, *3*, 732.
[3] W. Zhou, D. Zhu, J. He, J. Li, H. Chen, Y. Chen, D. Chao, *Energy Environ. Sci.* **2020**, 10.1039/D0EE01221A.
[4] T. M. Bandhauer, S. Garimella, T. F. Fuller, *J. Electrochem. Soc.* **2011**, *158*, R1.
[5] J. Kim, J. Oh, H. Lee, *Appl. Therm. Eng.* **2019**, *149*, 192.
[6] Q. Wang, P. Ping, X. Zhao, G. Chu, J. Sun, C. Chen, *J. Power Sources* **2012**, *208*, 210.
[7] X. Feng, M. Ouyang, X. Liu, L. Lu, Y. Xia, X. He, *Energy Storage Mater.* **2018**, *10*, 246.
[8] X. Feng, D. Ren, X. He, M. Ouyang, *Joule* **2020**, *4*, 743.
[9] J. Deng, C. Bae, J. Marcicki, A. Masias, T. Miller, *Nat. Energy* **2018**, *3*, 261.
[10] D. Chen, J. Jiang, G.-H. Kim, C. Yang, A. Pesaran, *Appl. Therm. Eng.* **2016**, *94*, 846.
[11] H. Li, F. Wang, C. Zhang, W. Ji, J. Qian, Y. Cao, H. Yang, X. Ai, *Energy Storage Mater.* **2019**, *17*, 275.
[12] Z. Chen, P.-C. Hsu, J. Lopez, Y. Li, J. W. F. To, N. Liu, C. Wang, S. C. Andrews, J. Liu, Y. Cui, Z. Bao, *Nat. Energy* **2016**, *1*, 15009.
[13] H. Yang, Z. Liu, B. K. Chandran, J. Deng, J. Yu, D. Qi, W. Li, Y. Tang, C. Zhang, X. Chen, *Adv. Mater.* **2015**, *27*, 5593.
[14] Y. Shi, H. Ha, A. Al-Sudani, C. J. Ellison, G. Yu, *Adv. Mater.* **2016**, *28*, 7921.
[15] J. Zhao, K. K. Sonigara, J. Li, J. Zhang, B. Chen, J. Zhang, S. S. Soni, X. Zhou, G. Cui, L. Chen, *Angew. Chem. Int. Ed.* **2017**, *56*, 7871.
[16] P. Zhang, J. Wang, W. Sheng, F. Wang, J. Zhang, F. Zhu, X. Zhuang, R. Jordan, O. G. Schmidt, X. Feng, *Energy Environ. Sci.* **2018**, *11*, 1717.
[17] Y. Yang, D. Yu, H. Wang, L. Guo, *Adv. Mater.* **2017**, *29*, 1703040.
[18] D. Yu, X. Li, J. Xu, *Sci. China Mater.* **2019**, *62*, 1556.
[19] D. Chao, W. Zhou, F. Xie, C. Ye, H. Li, M. Jaroniec, S.-Z. Qiao, *Sci. Adv.* **2020**, *6*, eaba4098.
[20] X. Gao, H. Zhang, X. Liu, X. Lu, *Carbon Energy* **2020**, *2*, 387.
[21] H. Zhang, Y. Fang, F. Yang, X. Liu, X. Lu, *Energy Environ. Sci.* **2020**, *13*, 2515.
[22] J. Liu, N. Nie, J. Wang, M. Hu, J. Zhang, M. Li, Y. Huang, *Mater. Today Energy* **2020**, *16*, 100372.
[23] L. Zhang, D. Chao, P. Yang, L. Weber, J. Li, T. Kraus, H. J. Fan, *Adv. Energy Mater.* **2020**, *10*, 2000142.
[24] M. Han, J. Zhi, T. K. A. Hoang, Y. Li, L. Li, P. Chen, *J. Power Sources* **2019**, *441*, 227171.
[25] F. Mo, H. Li, Z. Pei, G. Liang, L. Ma, Q. Yang, D. Wang, Y. Huang, C. Zhi, *Sci. Bull.* **2018**, *63*, 1077.
[26] J. Zhu, M. Yao, S. Huang, J. Tian, Z. Niu, *Angew. Chem. Int. Ed.* **2020**, *59*, 16480.
[27] P. Yu, Y. Zeng, H. Zhang, M. Yu, Y. Tong, X. Lu, *Small* **2019**, *15*, 1804760.
[28] J. A. Rard, D. G. Miller, *J. Chem. Thermodyn.* **1989**, *21*, 463.
[29] C. Yang, Z. Suo, *Nat. Rev. Mater.* **2018**, *3*, 125.
[30] W. Xie, J. Duan, H. Wang, J. Li, R. Liu, B. Yu, S. Liu, J. Zhou, *J. Mater. Chem. A* **2018**, *6*, 24114.
[31] S. Pu, J. Fu, Y. Liao, L. Ge, Y. Zhou, S. Zhang, S. Zhao, X. Liu, X. Hu, K. Liu, J. Chen, *Adv. Mater.* **2020**, *32*, 1907307.
[32] S. Pu, Y. Liao, K. Chen, J. Fu, S. Zhang, L. Ge, G. Conta, S. Bouzarif, T. Cheng, X. Hu, K. Liu, J. Chen, *Nano Lett.* **2020**, *20*, 3791.
[33] J. Lu, C. Zhan, T. Wu, J. Wen, Y. Lei, A. J. Kropf, H. Wu, D. J. Miller, J. W. Elam, Y.-K. Sun, X. Qiu, K. Amine, *Nat. Commun.* **2014**, *5*, 5693.
[34] P. Yang, H. J. Fan, *Chem. Res. Chin. Univ.* **2020**, *36*, 420.
[35] A. J. Dekker, *Ionic Conductivity and Diffusion* (Ed.: A. J. Dekker), Macmillan Education UK, London, **1981**, 160.

[36] W. Sun, F. Wang, S. Hou, C. Yang, X. Fan, Z. Ma, T. Gao, F. Han, R. Hu, M. Zhu, C. Wang, *J. Am. Chem. Soc.* **2017**, *139*, 9775.
[37] D. Chao, W. Zhou, C. Ye, Q. Zhang, Y. Chen, L. Gu, K. Davey, S. Z. Qiao, *Angew. Chem. Int. Ed.* **2019**, *58*, 7823.
[38] Y. Zeng, X. Zhang, Y. Meng, M. Yu, J. Yi, Y. Wu, X. Lu, Y. Tong, *Adv. Mater.* **2017**, *29*, 1700274.
[39] D. Wang, H. Li, Z. Liu, Z. Tang, G. Liang, F. Mo, Q. Yang, L. Ma, C. Zhi, *Small* **2018**, *14*, 1803978.
[40] F. Mo, G. Liang, Q. Meng, Z. Liu, H. Li, J. Fan, C. Zhi, *Energy Environ. Sci.* **2019**, *12*, 706.
[41] X. Guo, J. Zhou, C. Bai, X. Li, G. Fang, S. Liang, *Mater. Today Energy* **2020**, *16*, 100396.
[42] H. Liu, Z. Wei, W. He, J. Zhao, *Energy Convers. Manage.* **2017**, *150*, 304.
[43] H. S. Mansur, C. M. Sadahira, A. N. Souza, A. A. P. Mansur, *Mater. Sci. Eng., C* **2008**, *28*, 539.
[44] D. M. Price, *Thermochim. Acta* **2001**, *367-368*, 253.

A general self-adaptive strategy to circumvent the thermal runaway of zinc-ion batteries is presented by employing zinc chloride-enriched hygroscopic hydrogel electrolytes. Temperature changes cause water evaporation or absorption in the hydrogel, and then reversibly regulate the migration of ions in the hydrogel electrolyte, realizing the intelligent thermal self-protection of batteries.

**Keywords** zinc-ion battery, thermal self-protection, hygroscopic hydrogel, intelligent

P. Yang, C. Feng, Y. Liu, T. Cheng, X. Yang, H. Liu, K. Liu,* H. J. Fan*

**Thermal Self-Protection of Zinc-Ion Batteries Enabled by Smart Hygroscopic Hydrogel Electrolytes**

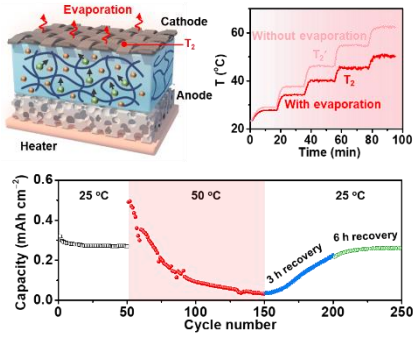

((Supporting Information can be included here using this template))



# Supporting Information

**Thermal Self-Protection of Zinc-Ion Batteries Enabled by Smart Hygroscopic Hydrogel Electrolytes**

*Peihua Yang, Chunzao Feng, Yipu Liu, Ting Cheng, Xuelong Yang, Huidong Liu, Kang Liu,* and Hong Jin Fan**

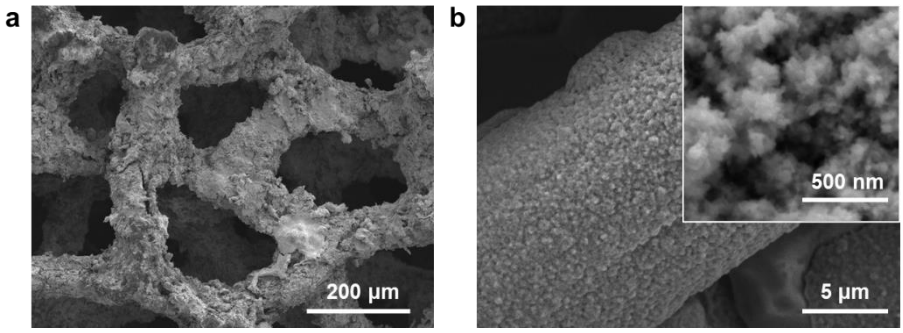


**Figure S1**. The SEM images of (a) zinc foam and (b) electrodeposited $MnO_2$ on carbon cloth fiber.

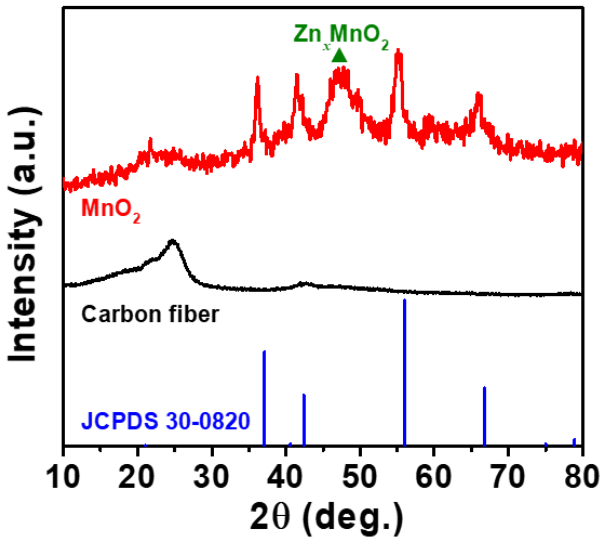


**Figure S2**. XRD patterns of the $MnO_2$ cathode, indicating the as-prepared sample is ε-phase $MnO_2$ (JCPDS 30-0820).

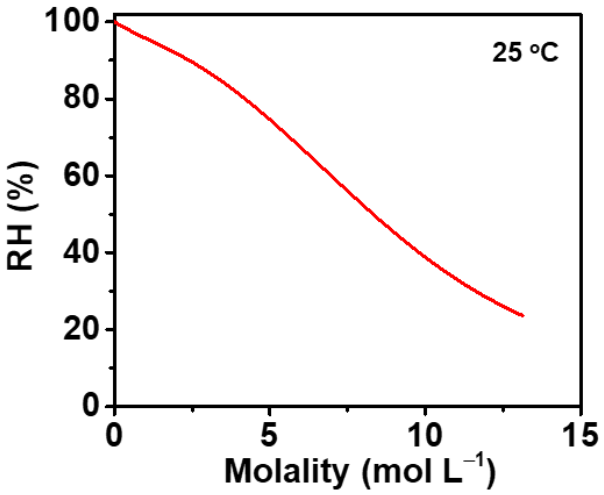


**Figure S3**. The saturated relative humidity of $ZnCl_2$ solution at 25 °C as a function of concentration (data collected from *J. Chem. Thermodyn.* **1989**, *21*, 463). The saturated relative humidity of 5.5 mol $L^{-1}$ $ZnCl_2$ solution is ~70% RH.

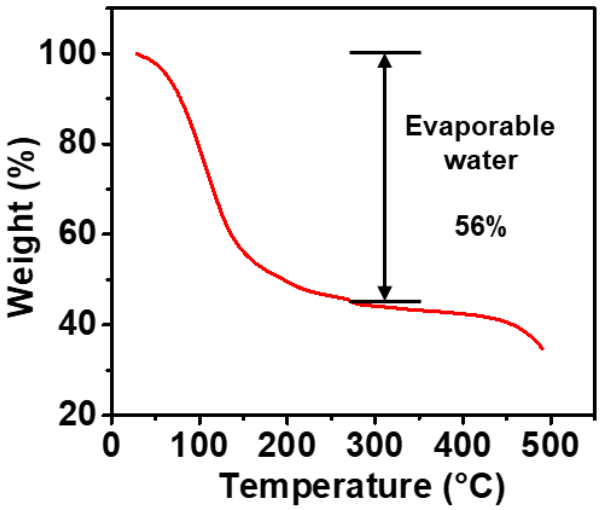


**Figure S4**. Thermogravimetric characterization of Zn-PAAm hydrogel, indicating that the vaporizable water in the hydrogel accounts for ~56% by weight of the total.

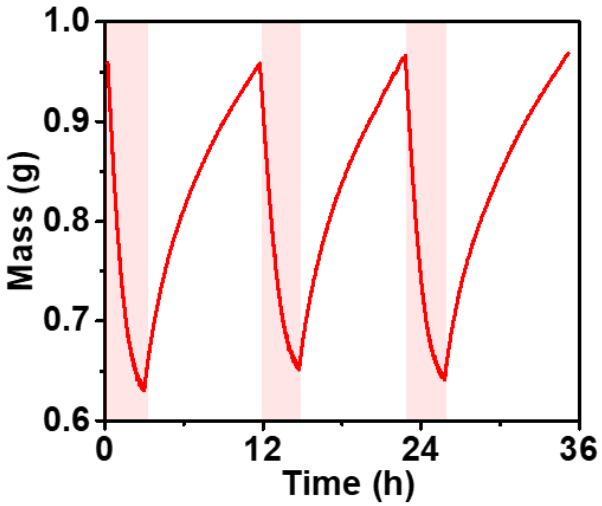


**Figure S5**. Mass variation of the Zn-PAAm hydrogel when the environment's relative humidity was 70%, and the temperature was periodically set at 50 °C (red shadow region) and 25 °C.

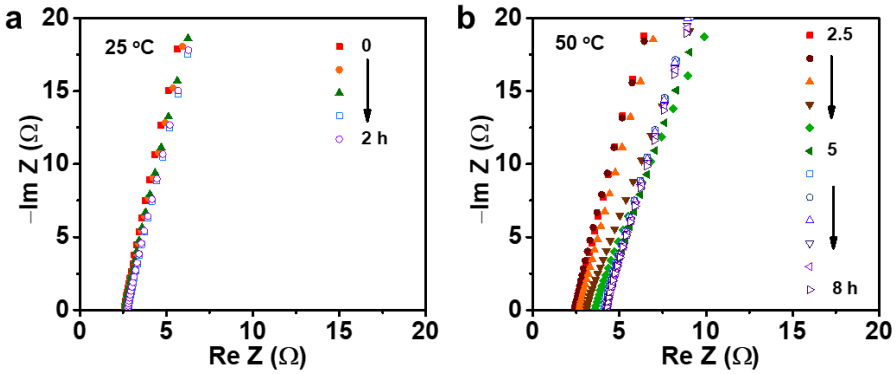


**Figure S6**. Conductivity and ions diffusion coefficient measurement using a Pt || Zn-PAAm || carbon fiber configuration under (a) 25 °C and (b) 50 °C. Each test interval is half an hour.

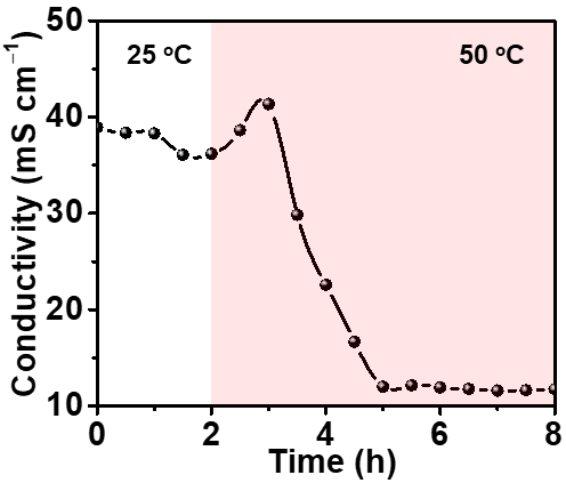


**Figure S7**. Conductivity of the hydrogel electrolyte when the temperature increased from 25 °C to 50 °C.

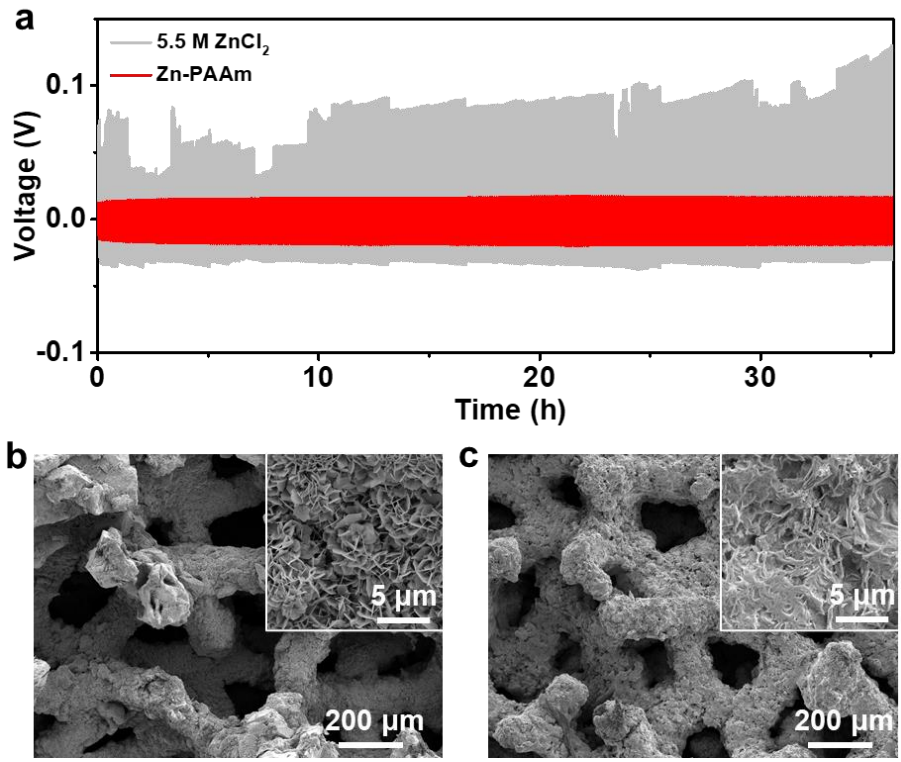


**Figure S8**. Stability of the zinc foam anode. (a) Galvanostatic plating/stripping curves of zinc symmetrical cells with different electrolytes at a current density of 5 mA cm$^{-2}$ and a cut-off capacity of 0.2 mAh cm$^{-2}$. (b-c) SEM images of zinc foam after galvanostatic plating/stripping cycling in (b) 5.5 mol L$^{-1}$ $ZnCl_2$ and (c) Zn-PAAm electrolytes.

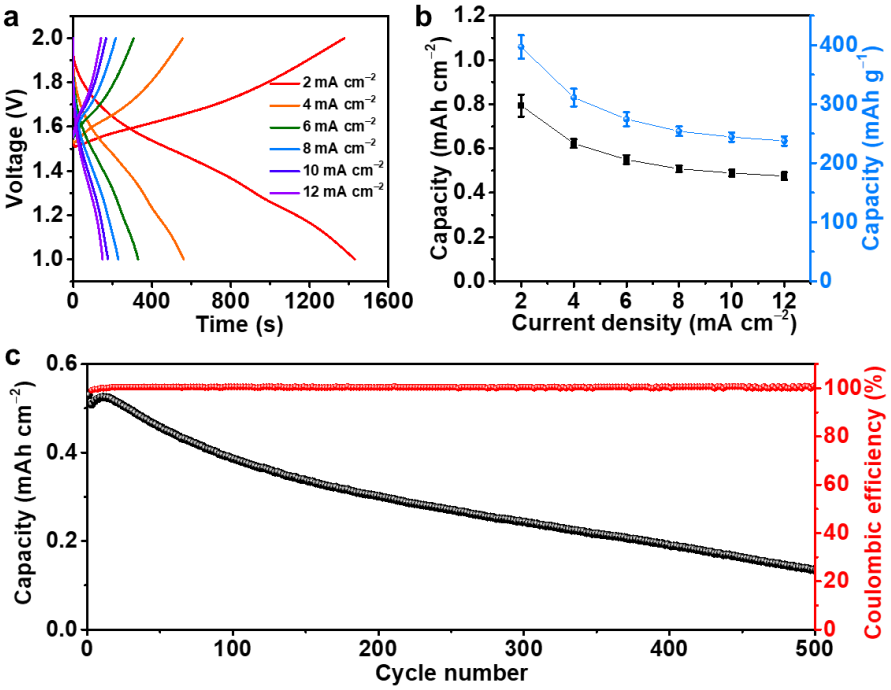


**Figure S9**. Electrochemical performance of zinc-ion batteries based on 5.5 mol $L^{-1}$ aqueous $ZnCl_2$ electrolyte at ambient condition. (a) The charge and discharge curves under different current densities. (b) Areal capacity and gravimetric capacity calculated based on discharge curves. Statistical analysis is based on four similar samples. (c) Cycling stability test at 10 mA $cm^{-2}$.

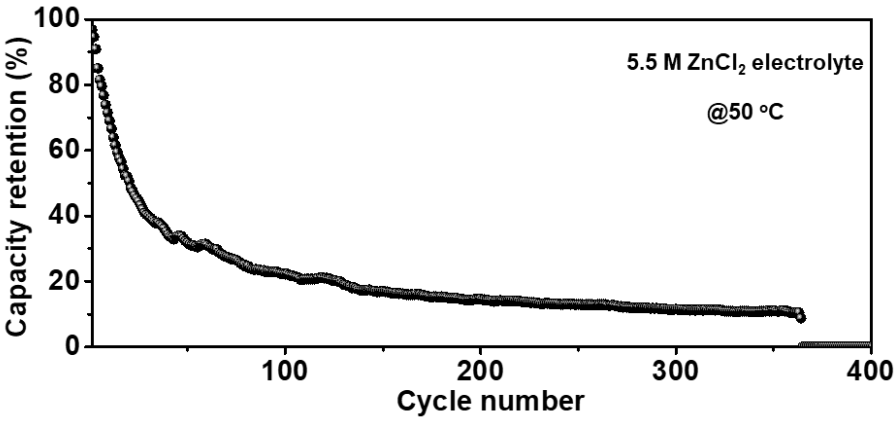


**Figure S10**. Cycling stability test at 10 mA $cm^{-2}$ of a zinc-ion battery based on 5.5 mol $L^{-1}$ $ZnCl_2$ electrolyte at 50 °C.

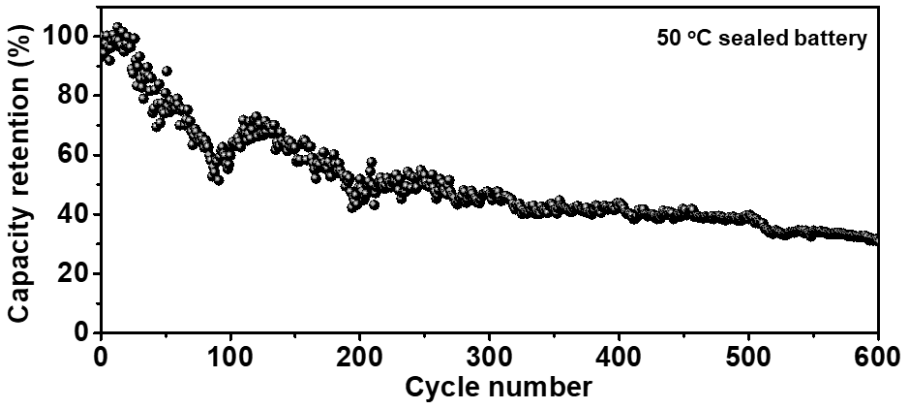


**Figure S11**. Cycling stability test at 10 mA $cm^{-2}$ of a sealed zinc-ion battery based on Zn-PAAm electrolyte at 50 °C.

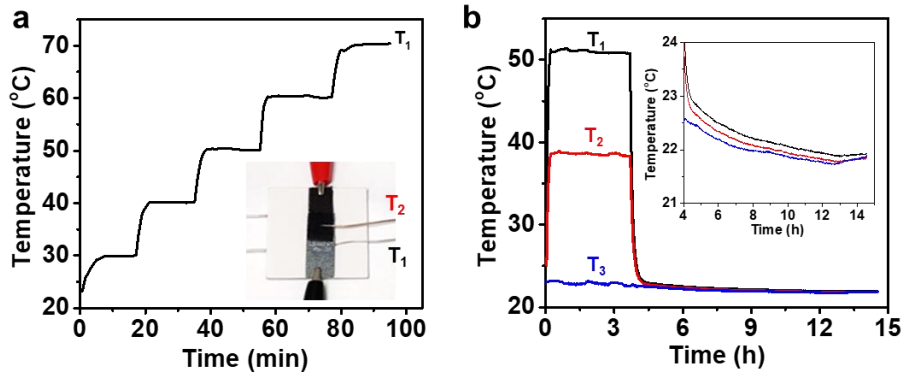


**Figure S12**. The temperature evolutions during water evaporation and regeneration. (a) The temperature evolution of the heater during transient heating. Inset shows a photograph of the setup. (b) The temperature of heater ($T_1$), cathode ($T_2$) and environment ($T_3$) when the hearter changes from on to off. Inset: enlarged view of the tail when the heater is switched off.

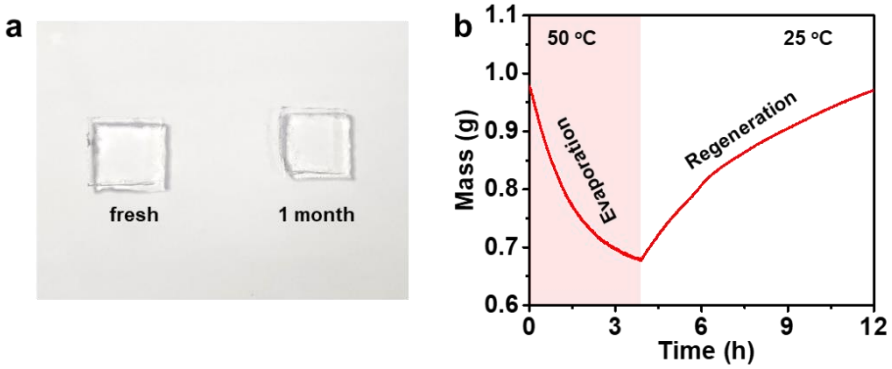


**Figure S13**. Characterization of the Zn-PVA hydrogel electrolyte. (a) Photograph of a piece of hydrogel which have been storaged in laboratory air ambient for one month and a piece of newly prepared hydrogel. The size of the samples is ~2 cm × 2 cm × 2 mm. (b) Mass change of the hydrogel at 50 °C and subsequent mass recovery at 25 °C.